

Electronic Supplementary Information

Microfluidic Passive Permeability Assay using Nanoliter Droplet Interface Lipid Bilayers

Takasi Nisisako,^{a,b} Shiva A. Portonovo,^a and Jacob J. Schmidt^a

^a*Department of Bioengineering, University of California, Los Angeles, CA, 90095-1600, U.S.A.*

^b*Precision and Intelligence Laboratory, Tokyo Institute of Technology, Yokohama, 226-8503, Japan*

1. Microfluidic channel characterization

For the characterization of the microfabricated grooves (Figs. S1 and S2), a scanning electron microscope (VE-8800, Keyence, Japan) was used. We also measured the 3D dimensions of the microgrooves by using a laser microscope (VK-9700, Keyence, Japan, **Fig. S2**).

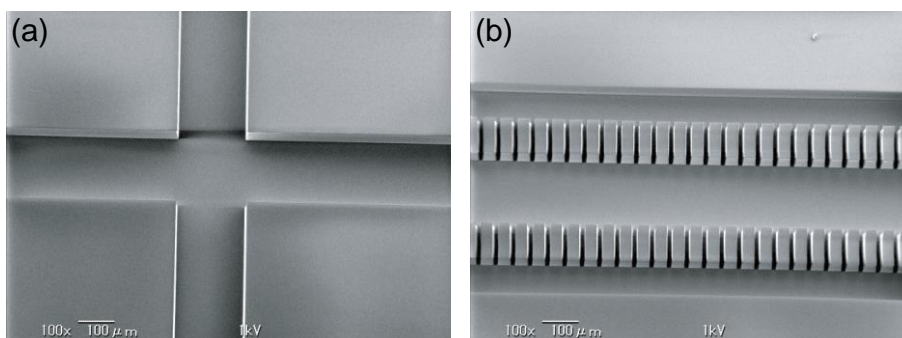


Figure S1. Scanning electron microscopy (SEM) images of the grooves fabricated by DRIE. (a) A cross junction (200 μm width) to produce donor and acceptor droplets alternately. (b) A main channel (200 μm width) with narrower sub channels (20 μm width, 30 μm gap) on the side walls to selectively aspirate the organic phase. The height of the grooves is uniformly 100 μm.

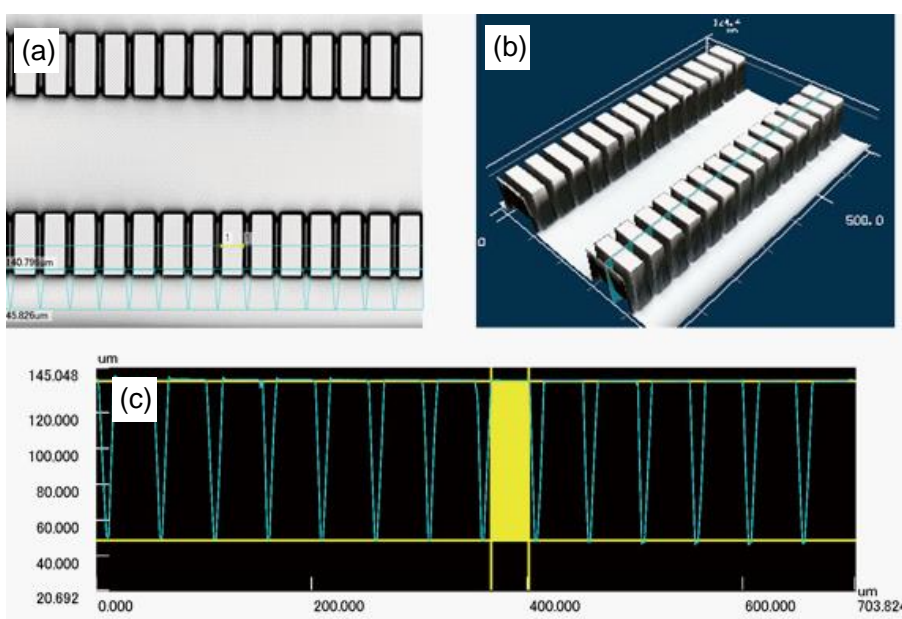


Figure S2. Optical measurement of 3D shape of the microfabricated grooves. (a) Top view of the main channel. (b) Optically measured 3D shape of the main channel. (c) A 2D profile of the pseudo-porous structure.

2. Calibration data for fluorescein permeability assay

Examples of calibration curves for fluorescein permeability assay are given in **Fig. S3**.

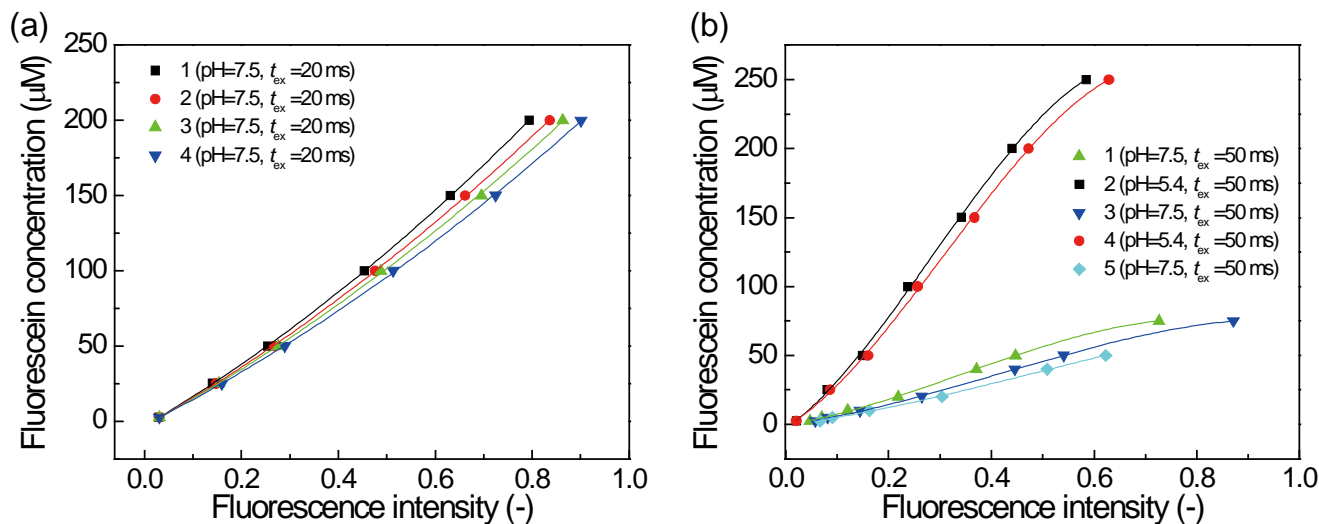


Figure S3. Calibration curves for fluorescein permeability assays. (a) Four calibration curves for the four-droplet array with two donor droplets at pH 7.5 and two acceptor droplets at pH 7.5 (Fig. 3). Positions 1 and 3 correspond to the positions of AD1 and AD2 in Fig. 3. Positions 2 and 4 correspond to the positions of DD1 and DD2 in Fig. 3. (b) Five calibration curves for the five-droplet array with two donor droplets at pH 5.4 and three acceptor droplets at pH 7.5 (Fig. 4). Positions 1, 3, 5 correspond to the positions of AD1, AD2, and AD3 in Fig. 4. Positions 2 and 4 correspond to the positions of DD1 and DD2 in Fig. 4.

3. Fluorescein permeation across hexadecane

Figure S4a is an array of four droplets comprised of two donor droplets at pH 5.4 and two acceptor droplets at pH 7.5, where an acceptor droplet (AD1) is separated from the other three droplets. When we fluorometrically measured the time-dependence of change of fluorescein concentration in the droplets, we observed the increase of intensity in both separated (AD1) and attached (AD2) acceptor droplets due to uptake of fluorescein molecules (**Fig. S4b**), although we found that the rate of increase in AD1 is much slower than AD2 (**Fig. S4c**). This result clearly shows that fluorescein molecules can partition into the bulk hexadecane phase.

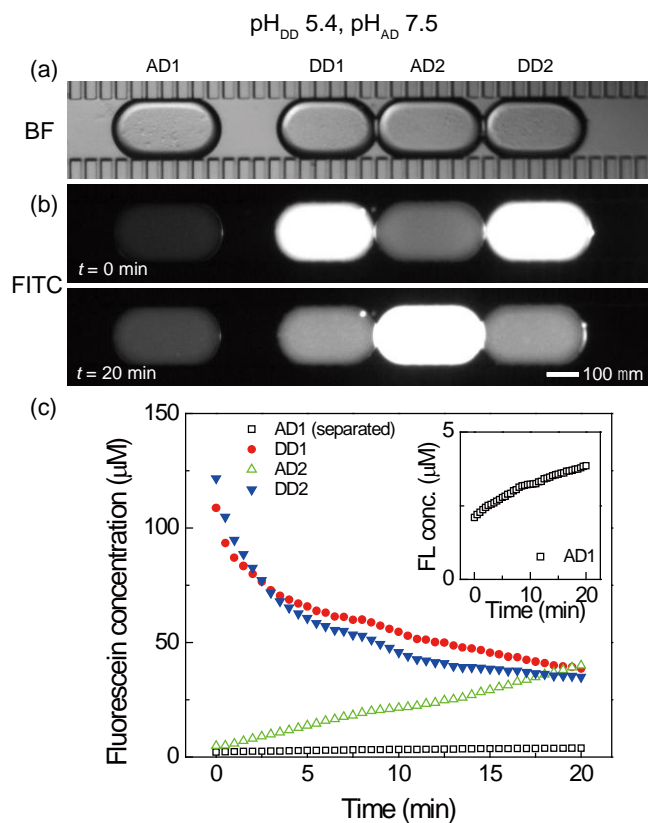


Figure S4. Measurement of fluorescein permeation across hexadecane. (a) A bright field microscopy image of the four droplet array in which two donor droplets (DD1 and DD2, pH 5.4) and an acceptor droplet (AD2, pH 7.5) are in contact and a single acceptor droplet (AD1, pH 7.5) is separated from the others. (b) Time-lapse fluorescent microscopy images at start and end of the measurements. (c) Measured variation of fluorescein concentrations in droplets over time. The inset shows the increase of fluorescein concentration in AD1.

4. A permeation model to calculate effective permeability

To obtain the effective permeability of a solute, diffusion-based permeation in an array of n aqueous droplets surrounded by oil (**Fig. S5**) can be described by a set of $n+1$ simultaneous ordinary differential equations and a mass-conservation equation as below:

$$V_1 \frac{dC_1}{dt} = k_1(C_2 - C_1) + k_n(C_{n+1} - C_1) \quad (1)$$

$$V_i \frac{dC_i}{dt} = k_{i-1}(C_{i-1} - C_i) + k_i(C_{i+1} - C_i) + k_{n+i-1}(C_{n+1} - C_i) \quad (2)$$

$$V_n \frac{dC_n}{dt} = k_{n-1}(C_{n-1} - C_n) + k_{2n-1}(C_{n+1} - C_n) \quad (3)$$

$$V_{n+1} \frac{dC_{n+1}}{dt} = k_n(C_1 - C_{n+1}) + \dots + k_{n+i-1}(C_1 - C_{n+1}) + \dots + k_{2n-1}(C_n - C_{n+1}) \quad (4)$$

$$V_1C_1 + V_2C_2 + \dots + V_{n+1}C_{n+1} = \text{Const.} \quad (5)$$

where V_1, \dots, V_n are droplet volumes, C_1, \dots, C_n are the total concentrations of the solute (of all charge-state forms) in the droplets, V_{n+1} is the volume of organic phase, C_{n+1} is the total concentration of the solute in the organic phase. The effective permeability of each membrane $P_{e,i}$ is given by $P_{e,i} = k_i / S_i$ where S_i is the area of membrane.

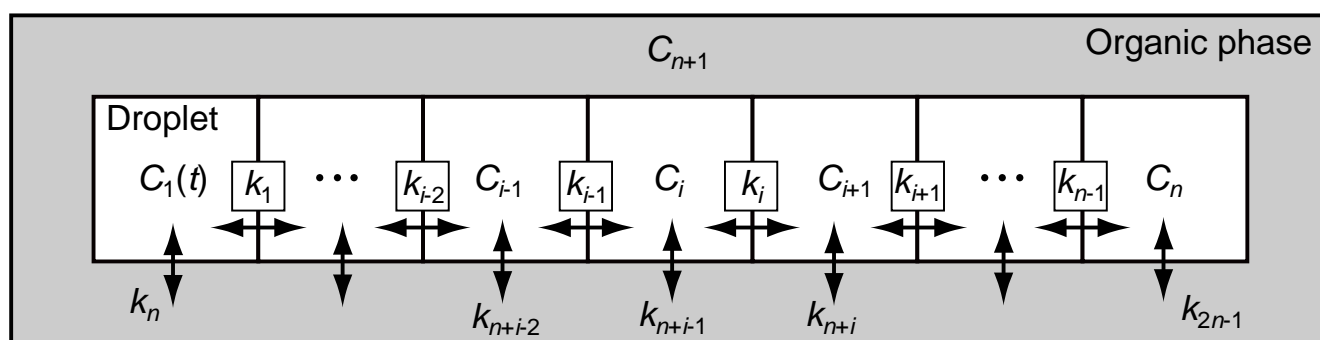


Figure S5. A multi-box model to describe permeation in arrayed n aqueous droplet surrounded by an external organic phase.

5. Enhanced permeation model to calculate intrinsic permeabilities of differently charged permeants

Figure S6 is a model to obtain intrinsic permeabilities for each of four differently charged forms of fluorescein molecules. C_1 , C_2 , and C_3 are the total concentration of fluorescein in droplet 1, droplet 2, and external organic phase. $C_{(+)}$, $C_{(0)}$, $C_{(-)}$, $C_{(2-)}$ are the concentration of monocations, uncharged molecules, monoanions, and dianions in each phase, which can be calculated by the Henderson-Hasselbalch equations. $k_{(+)}$, $k_{(0)}$, $k_{(-)}$, and $k_{(2-)}$ are the permeation rate coefficient of monocations, uncharged molecules, monoanions, and dianions. For example, a differential equation for the variation of the amount of molecules in droplet 1 is described as below:

$$\begin{aligned}
 V_1 \frac{dC_1}{dt} = & k_{1(+)}(C_{2(+)} - C_{1(+)}) + k_{2(+)}(C_{3(+)} - C_{1(+)}) \\
 & + k_{1(0)}(C_{2(0)} - C_{1(0)}) + k_{2(0)}(C_{3(0)} - C_{1(0)}) \\
 & + k_{1(-)}(C_{2(-)} - C_{1(-)}) + k_{2(-)}(C_{3(-)} - C_{1(-)}) \\
 & + k_{1(2-)}(C_{2(2-)} - C_{1(2-)}) + k_{2(2-)}(C_{3(2-)} - C_{1(2-)})
 \end{aligned} \tag{6}$$

Intrinsic permeability P_0 of each form is given by $P_{0,i} = k / S_i$, where S_i is the area of membrane. The other differential equations for droplet 2 and organic phase can be described as well and these equations were easily enhanced for n -droplet array as shown in Fig. S5. We used this model to obtain intrinsic permeabilities of monoanion $P_{0(-)}$ and neutral species $P_{0(0)}$ of fluorescein. First, we simplified these equations by setting $C_{(+)}$ to 0 and assuming that $k_{(2-)}$ was 0. Then, we searched optimal $k_{(-)}$ values (and $P_{(-)}$ values) using above-mentioned optimization program and experimental data with donor droplets at pH 7.5, in which $C_{(0)}$ in the equations could be set to be 0. The obtained values were then used with experimental data with donor droplets at pH 5.4 and 6.4 to find optimal values of $k_{(0)}$ values (and $P_{(0)}$ values).

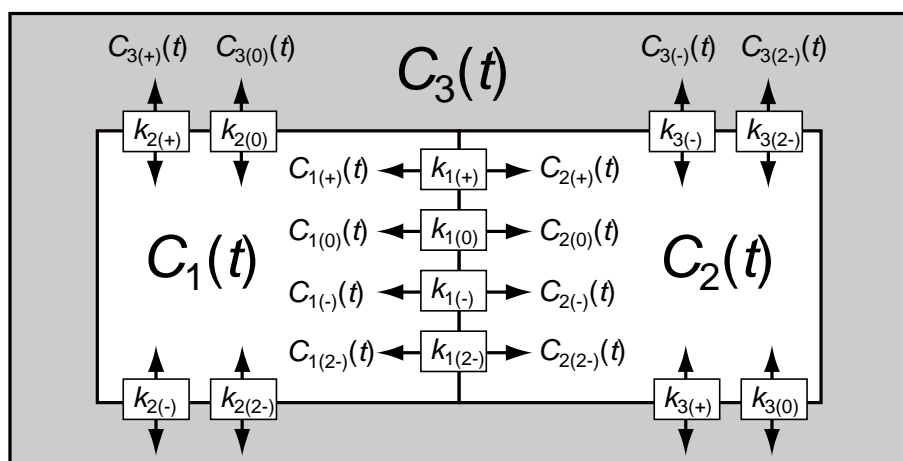


Figure S6. A two-box model to obtain intrinsic permeabilities of four differently charged fluorescein molecules.

6. Numerical calculation of permeability coefficients

Numerically solving for the permeation constants involved solving both sides of the system of differential equations listed in the paper. The differential term $\frac{dC}{dt}$ was calculated using the central difference formula, with concentration values from 2 time points as

such: $\frac{\Delta(\text{Concentration}_{\text{time}_{x+1}} - \text{Concentration}_{\text{time}_{x-1}})}{2 * \Delta(\text{time}_{x+1} - \text{time}_x)}$. The other parts of the equation could be calculated arithmetically. A cost function evaluated the equality condition of the right and left sides of the equations for various values of rate constants k and assigned incrementally favorable outcomes for incremental changes in k that brought the system closer to equality. Increment sizes on each k value were specified to be 0.0001. An optimization algorithm based on golden-section search supplied incremental changes to k values that successively brought right and left sides of the system of differential equations closer to equality. After settling on optimized k values from the program results, we could then obtain permeability values.

7. Calibration data for caffeine permeability assay

Figure S7 shows a set of calibration data for the caffeine permeability assay using UV-Vis microspectroscopy.

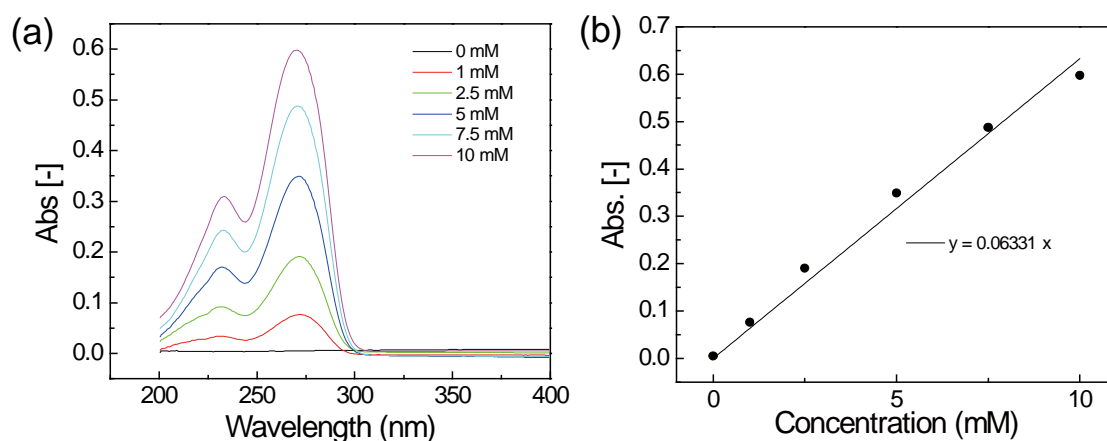


Figure S7. Calibration data for caffeine permeability assay. (a) Spectra of caffeine solutions with different concentrations (0, 1, 2.5, 5, 7.5, and 10 mM) in the wavelength range of 200–400 nm. (b) A calibration curve obtained from absorption peaks at 270 nm in (a).

8. Possible improvements in channel design to control and constrain droplet contact area

Standardization of the droplet contact area would greatly simplify and speed determination of permeabilities. **Fig. S8** shows a schematic of a modified channel design containing bumps protruding into the channel. If the droplets were injected into the channel so that they contact each other at locations in the channel containing the protruding bumps, the contact area is constrained.

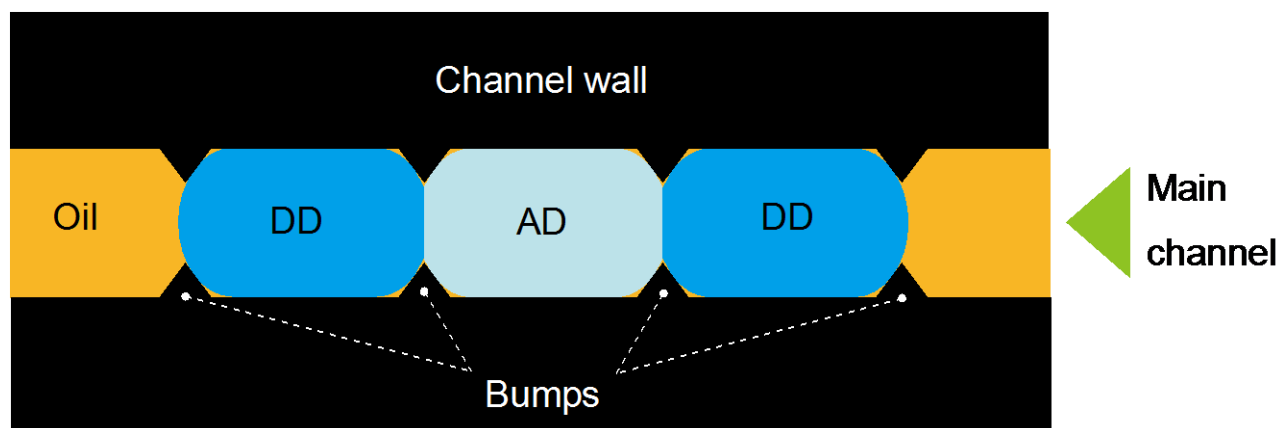


Figure S8. A schematic of a modified channel design containing bumps to control and constrain droplet contact area.